Chapter 33
Coupled Vibro-Acoustic Model of the *Titian* Stradivari Violin

Michael A. Pyrkosz and Chuck Van Karsen

Abstract The instruments of Antonio Stradivari (1644–1737) are still considered the finest in the world and have set the standard for violin quality that has yet to be exceeded by a modern luthier. To determine the relationship between the sound of the instrument and its structure and material properties a vibro-acoustic finite element model was developed for the 1715 *Titian* Stradivari violin. The structural model was created by measuring the structural geometry and density from CT scans of the actual instrument. The predicted structural modes were correlated with experimental modal data on the 1715 violin and updated accordingly. The correlated structural modes were then projected onto the acoustic envelope. The vibro-acoustic transfer function between force input at the violin bridge and acoustic pressure response 1.2 m away was predicted. These results were compared to experimental radiativity measurements made on the actual instrument. It was shown that including structural and acoustic damping characteristics are important to accurately predict the vibro-acoustic behavior of the *Titian* Stradivari violin. Predicted structural modal frequencies were all within 5 % of the experimental data, while the main acoustic mode was within 7 %. The predicted radiativity magnitude was within 1.5 dB for all mode peaks. This is the first comprehensive analytical vibro-acoustic model of a Stradivari instrument and can be used to determine how structural modifications effect violin sound quality.

Keywords Vibro-acoustic coupling • Finite element acoustics • Model validation • Violin acoustics • Antonio Stradivari

Nomenclature

c	Speed of sound
k	Wave number
MAC	Modal assurance criterion
p	Acoustic pressure
r	Acoustic field position vector
t_{PML}	Thickness of the perfectly matched layer
V	Mode shape vector
ζ	Damping factor, $\zeta = C/Cc$
η	Loss factor, energy dissipation per cycle
λ	Wave length, $\lambda = 1/f = 2\pi/\omega$
ρ	Mass density

M.A. Pyrkosz (✉)
LMS, A Siemens Business, Engineering Services, LMS North America, 5755 New King Court, Troy, MI 48098, USA
e-mail: Mike.Pyrkosz@lmsintl.com

C. Van Karsen
Dynamic Systems Laboratory, Mechanical Engineering-Engineering Mechanics, Michigan Technological University, 1400 Townsend Drive, Houghton, MI 49931, USA

J. De Clerck (ed.), *Topics in Modal Analysis I, Volume 7: Proceedings of the 32nd IMAC, A Conference and Exposition on Structural Dynamics, 2014*, Conference Proceedings of the Society for Experimental Mechanics Series,
DOI 10.1007/978-3-319-04753-9_33,

33.1 Introduction

Today, the instruments made by Antonio Stradivari in the early eighteenth century are considered to be the best in the world. Unfortunately, no one in our generation fully understands how Stradivari crafted his instruments, and no one has ever produced an instrument that has quite the same musical quality of one of his instruments. There are many theories about how Stradivari made his instruments, and why they are superior to other violins. To determine the relationship between the sound of the instrument and its structure and material properties a vibro-acoustic finite element model was developed for the 1715 *Titian* Stradivari violin. The structural model was created by measuring the structural geometry and density from CT scans of the actual instrument [1].

The next step is to bring the dynamic behavior of the structural model in greater agreement with the real test structure through modal correlation and updating. This technique uses correlation of experimental modal data with the modal results of an approximate FE model with initial material properties. The sensitivity of the correlation to the different properties is determined and the material properties are updated accordingly. This process is iterated until the model is a reasonable representation of reality.

The final step in the process was to create an accurate vibro-acoustic model of the instrument. To do this an acoustic finite element mesh was developed based on the existing structural FE model. The predicted structural modes were projected onto this mesh, and a coupled vibro-acoustic analysis was performed to predict the transfer function between acoustic pressure response and force input at the violin bridge. These results were compared to experimental radiativity measurements made on the actual instrument [2–4]. The acoustical model properties were updated accordingly. The structural and acoustic damping properties were both found to play an important role in vibro-acoustic response.

33.2 Methods

33.2.1 Model Methods

The basic modeling methods employed in this project were thoroughly discussed in an earlier publication [1]. The following is a summary. Geometry and density information is taken from CT scans of the actual instrument. The CT images are taken through a CT interpretation program where the various parts are converted into 3D objects and surface meshed. The meshes are exported to a Finite Element (FE) format and edited in a FE preprocessor. These surface meshes envelope the original 3D objects computed by the CT interpretation software. For thin parts, such as the plates and ribs, the surface mesh is reduced to a single layer on the outer surface. For solid parts, such as the blocks, and the neck and scroll, the original surface mesh is filled with solid elements.

The triangular elements generated on the surfaces by the CT interpretation software were upgraded to quadrangular elements for improved performance. Care was taken to match opposing faces of solid components (i.e. blocks, sound post, bass bar, neck and scroll) so that they could be filled with hex-dominant meshes. Figure 33.1 shows a side-by-side comparison of the mid-treble region of the corpus before and after the re-meshing process. Note that the edges around plates and f-holes are now smooth.

Strings were modeled with a series of beam elements between the bridge and the nut (128 elements each) and between the bridge and the tail piece (20 elements each). The windings on the G, D, and A strings were modeled as non-structural mass. Properties for the beam elements were taken from those used in Knott's model [5]. Similarly, the tail loop is modeled as two lines of beam elements between the bottom of the tail piece and the saddle (three elements each).

To apply tension in the strings a static preload subcase was included. At the top of each string a coincident node was added at the string-nut interface and connected with a zero-length rigid bar element (RBE). In this way a local axis system could be created for each string to orient the DOF of the RBE with that of the beams. The constraint in the axial direction was then excluded for each RBE. Initial preloads were applied in the axial direction at each of the beams. After an initial run, these tension preloads were adjusted to "tune" the stings.

The final *Titian* Stradivari violin structural FE mesh contains 74,756 nodes and 117,528 elements. A full description of the *Titian* Stradivari mesh composition is given in Table 33.1. Note that skins are not included in the individual component counts but are included in the full mesh. The plates were attached to the rib structure with a single layer of hexahedral elements. Figure 33.2 shows a screen capture of the final *Titian* Stradivari FE mesh.

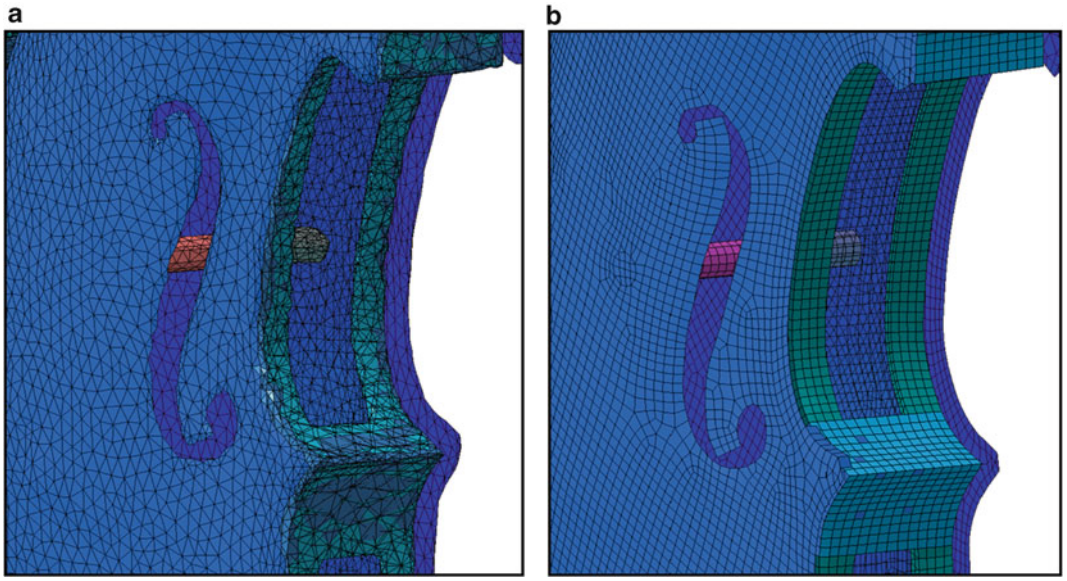

Fig. 33.1 Comparison of the mid-treble region of the corpus (**a**) before and (**b**) after the remeshing

Table 33.1 *Titian* Stradivari violin structural FE mesh composition

Component	Beams	TRIA	QUAD	TETRA	PENTA	HEXA	Total elements (no skins)
Back plate	–	62	11,193	–	–	–	11,255
Top plate + bass bar	–	46	10,619	186	18	1,176	12,045
Rib structure	–	–	6,458	–	266	10,724	17,448
Sound post	–	–	–	–	116	348	464
Neck and scroll	–	–	–	27,828	159	7,502	35,489
Fingerboard	–	–	–	–	–	4,032	4,032
Bridge	–	–	–	–	30	1,300	1,330
Tail piece	–	–	–	–	64	4,776	4,840
Nut	–	–	–	–	–	72	72
Saddle	–	–	–	–	–	84	84
Strings + tail loop	598	–	–	–	–	–	598
Full mesh (including skins)	598	438	55,526	28,014	691	32,206	117,528

The thickness graduations of both plates were mapped similarly to the factory violin, using the data collected by Zygmuntowicz and mapped by Loen [6]. The published graduation measurements were transferred to the coordinates of the model through a set of transformation vectors estimated from points taken at the corners. The results of the thickness mapping are shown in Figs. 33.3 and 33.4 (color (gray scale) indicates thickness in mm).

33.2.2 Structural Correlation Methods

Ensuring reliable validity of an FE model is essential for realistic noise and vibration simulations of penetrator systems. This requires that component, subsystem, and full-system models be compared to experimental data or to validated models of similar structures. One common tool for comparing and validating an FE model with experimental data is the Modal Assurance Criterion (MAC).

The modal assurance criterion is a statistical indicator that measures the degree of relationship between a pair of vectors [7]. These vectors can be the Modal vectors (normal or complex mode shapes) or Response vectors from a Forced

Fig. 33.2 Final *Titian* Stradivari violin structural FE model with Pre-loaded strings

Response Case for instance. The MAC values are normalized by the magnitude of the vectors, and thus always lie between 0 and 1, where values near 1 indicate consistency between the vectors, while values near 0 indicate the vectors are not consistent [7]. Generally, reasonable values of MAC are 0.7 whereas good correlation is above 0.9 [8].

The MAC formula between two vectors (V_i, V_j) is given in Eq. (33.1).

$$MAC_{ij} = \frac{\left[{V_i}^T \cdot V_j\right]^2}{\left[{V_i}^T \cdot V_i\right] \cdot \left[{V_j}^T \cdot V_j\right]} \tag{33.1}$$

Between an FE and test model this results in Eq. (33.2).

$$MAC_{Test_i FE_j} = \frac{\left[{V_{Test_i}}^T \cdot V_{FE_j}\right]^2}{\left[{V_{Test_i}}^T \cdot V_{Test_i}\right] \cdot \left[{V_{FE_j}}^T \cdot V_{FE_j}\right]} \tag{33.2}$$

More details on the modal assurance criterion can be found in [7, 8].

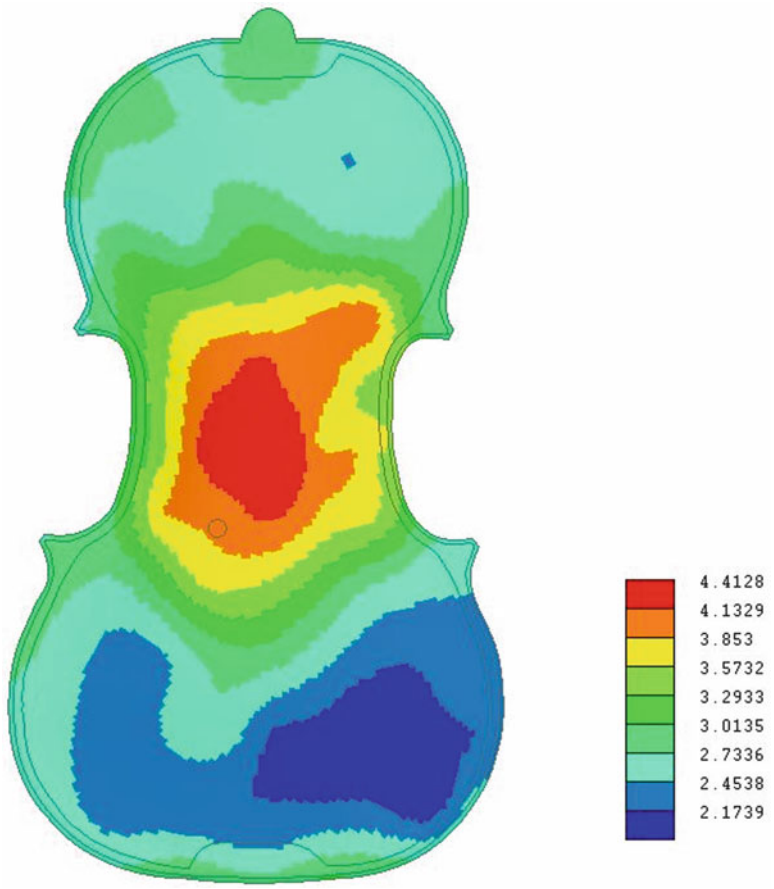

Fig. 33.3 Element thickness of the *Titian* Stradivari violin back plate in mm

33.2.3 Acoustic Methods

33.2.3.1 Sommerfeld Radiation Condition in FEM

Traditionally, the only practical way to handle an interior/exterior acoustic problem (such as a violin with an inner cavity connected to the outside air via the f-holes) was using the Boundary Element Method (BEM). However, technology has been developed in recent years that makes the Finite Element Method (FEM) more practical, and indeed better suited for the violin acoustic problem.

The Sommerfeld radiation condition requires that the boundary surface of the acoustic FEM mesh allows all acoustic waves to propagate freely towards infinity, and that no reflections occur at this boundary [9]. This is represented by Eq. (33.3).

$$\lim_{|\vec{r}|\to\infty} \left|\vec{r}\right| \cdot \left(\frac{\partial p\left(\vec{r}\right)}{\partial \left|\vec{r}\right|} + jkp\left(\vec{r}\right) \right) = 0 \tag{33.3}$$

There are currently two methodologies for handling the Sommerfeld radiation condition in exterior FEM problems: the Infinite Element Method (IFEM), and the Perfectly Matched Layer (PML).

IFEM is the older of these two, which requires that the boundary surface of the air be meshed as a canonical shape (such as a sphere or ellipsoid). Special decay shape functions are used on the boundary elements to minimize reflections. The radius of the boundary surface must be at least a full wavelength for the lowest frequency of interest, $R > \lambda$, and up to two full wavelengths away from radiating bodies. This leads to extremely large models with many elements to have a useful dynamic range.

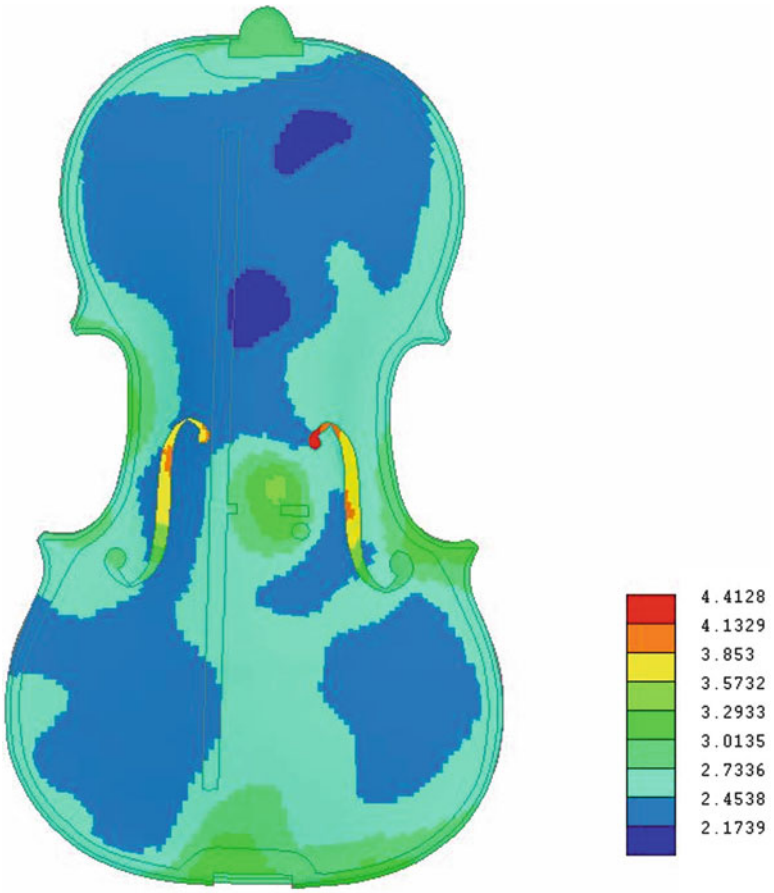

Fig. 33.4 Element thickness of the *Titian* Stradivari violin top plate in mm

With PML a special perfectly matched layer of elements is added to the outer boundary of a convex mesh that is locally-conformal to the structure mesh. This layer utilizes an anti-reflection function to create a coating around the radiating body to absorb the waves. In this case the thickness of the PML only needs to be greater than one fifteenth of the lowest frequency wavelength, $t_{PML} > (1/15)^* \lambda$. Additionally, the distance between the radiating surface and the boundary of the PML only needs to be one to two elements thick.

In both IFEM and PML response points may be placed inside or outside of the FEM boundary. For responses outside the FEM domain the solver will use Kirchoff surface integration to compute the solution for these points once the FEM solution is known.

33.2.3.2 Acoustic Mesh for FEM with AML

LMS Virtual.Lab (R11) software now includes an Automatically Matched Layer (AML) property. This feature constructs the absorbing layer on the solver level by extruding the boundary surface elements automatically [10]. This is similar to PML except that the layer is created on the solver level. This eliminates the need for the user to create the layer manually within the GUI.

For an opened structural mesh, the acoustic medium is present on both sides of the structure, and a volumize mesher was used to create duplicated meshes projected on both sides of the structural shell elements. This is shown in Fig. 33.5. The structure mesh of the violin is shown in green (gray in print version) (lines represent shell elements and filled-in areas represent solid elements). The volumize mesh is shown as a black line enveloping the structure mesh. The convex mesh is then created to wrap around the outside of the volumize mesh with room for at least one or two elements in between. The AML property is applied on this surface. A tetrahedron filler mesh is used to fill the space between the volumize mesh and the convex mesh with tetrahedral elements.

It should be noted that although the structural mesh must be fine to capture the bending waves through the wood materials, the acoustic mesh can be considerably coarser. By coarsening the acoustic mesh, the size of the model was kept small,

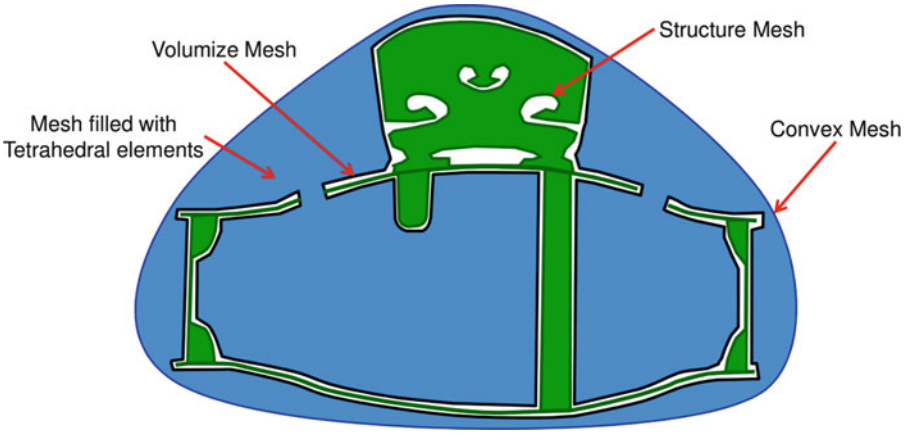

Fig. 33.5 Setting up FE meshes for AML property on an opened structural mesh of a violin

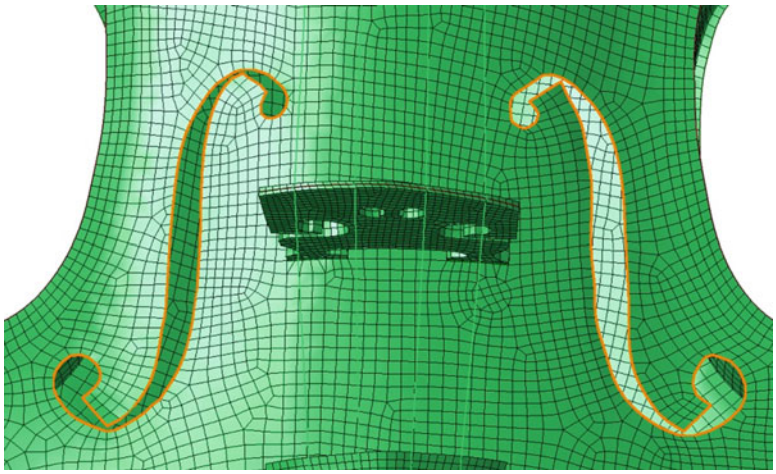

Fig. 33.6 The edges around the f-holes are selected to be maintained

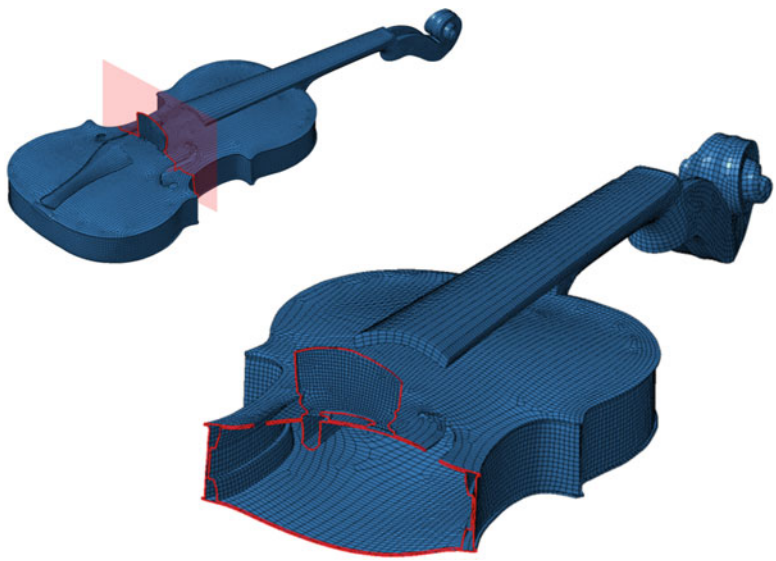

Fig. 33.7 Final volumize mesh of the *Titian* Stradivari violin and cut-plane at bridge location

reducing the solve time. This coarsening is performed before the volumize step. To ensure that the area around the f-holes is not compromised the edges of the f-holes are selected and a mesh group is created to maintain these edges during the coarsening process. This is shown in Fig. 33.6.

The final volumize mesh is shown in Fig. 33.7. This mesh is composed of 56,147 nodes, and 56,234 shell elements (56064 QUAD, and 170 TRIA). A cut-plane view of the final volumize mesh is also shown in Fig. 33.7. This mesh will become the "acoustic envelope" where the structural modes will be transferred to the surrounding air.

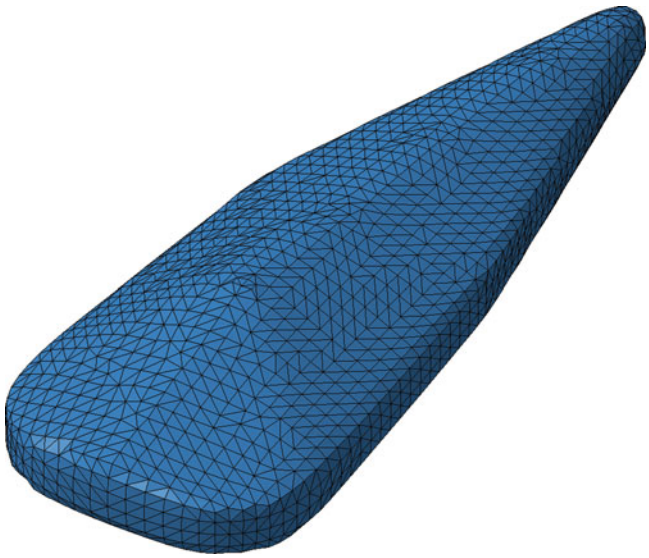

Fig. 33.8 Convex mesh around *Titian* Stradivari violin FE model

Table 33.2 Mesh compositions for vibro-acoustic FEM analysis of the *Titian* Stradivari violin

Structure mesh	Acoustic mesh
74,756 nodes	226,142 nodes
438 TRIA3 elements	1,191,283 TETRA4 elements
55,526 QUAD4 elements	
28,014 TETRA4 elements	
691 PENTA6 elements	
32,206 HEXA8 elements	
598 beam elements	
55 rigid spider elements	

A convex mesh was created around the volumize mesh. A scaling factor of 1.1 was applied, and the element size was set to 14 mm (this guarantees at least six elements per wavelength up to a frequency of 4,000 Hz, assuming speed of sound 340 m/s). The final convex mesh for the *Titian* Stradivari violin vibro-acoustic model is shown in Fig. 33.8. This mesh defines the point at which the AML property is applied.

Once a convex mesh was wrapped around the outside of volumize mesh the volume between the meshes was filled with tetrahedral elements.

The final mesh compositions of both the structure mesh and acoustic mesh are given in Table 33.2. Figure 33.9 shows the structural mesh inside a cut-away view of the acoustic mesh.

33.2.3.3 Coupled Vibro-Acoustic Set-Up

Once the acoustic mesh was prepared, several pre-processing steps were performed. These include setting the properties for air, defining the AML property on the convex mesh, transferring the structural modes onto the acoustic envelope, and defining input and output locations for the Vibro-acoustic transfer function analysis case.

Properties of air were initially assumed as follows:

Speed of Sound = 340 m/s
Mass density = 1.225 kg/m^3

The parameters used for the AML property are given in Table 33.3.

Response locations for the vibro-acoustic transfer function analysis were selected using field point meshes. These virtual microphones can be placed anywhere in the model. To create results comparable to the available experimental data [2], a spherical field point mesh was placed around the *Titian* Stradivari vibro-acoustic mesh. Like the Bissinger experiment its center point was set on the top plate, midway between the two bridge feet. The radius of the sphere was set to 1.2 m, and the number of equatorial elements was set to 24, creating a response location every 15° along the equator. The resulting sphere contained 218 nodes and is shown in Fig. 33.10.

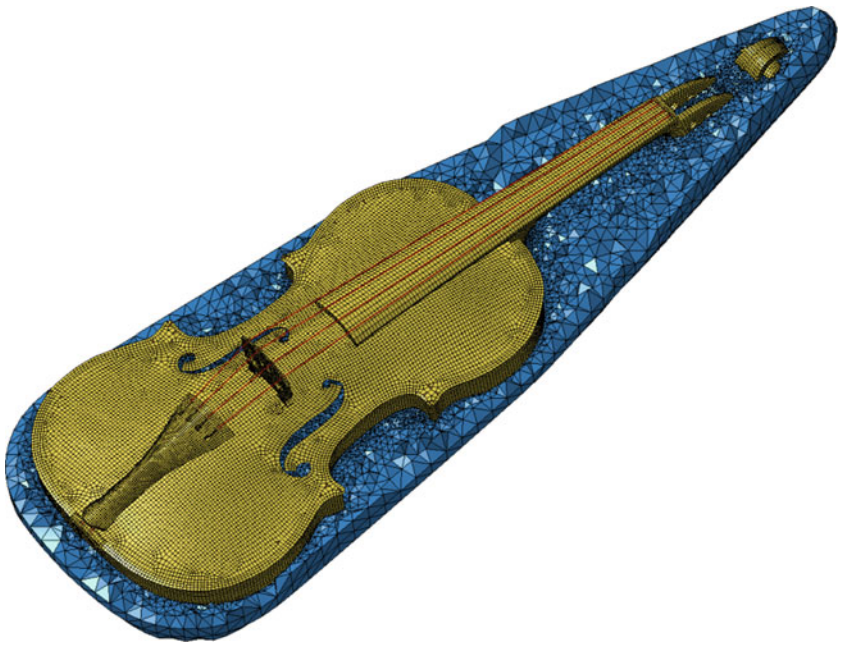

Fig. 33.9 *Titian* Stradivari structural FE mesh inside a cut-away (coronal) of the acoustic volume mesh

Table 33.3 AML parameters for vibro-acoustic analysis of the *Titian* Stradivari

Number of layers	5
Minimum thickness (as a ratio of wavelength)	0.16
Surface element count	3,728

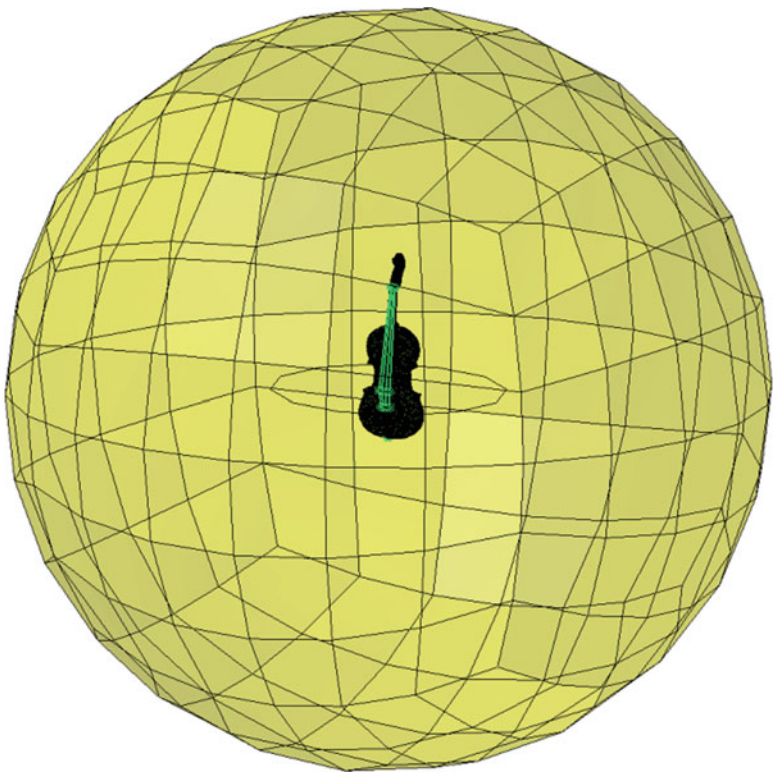

Fig. 33.10 Field point mesh around the *Titian* Stradivari FE model

Fig. 33.11 Input locations for the vibro-acoustic transfer function analysis of the *Titian* Stradivari violin

Five input locations were selected for the vibro-acoustic transfer function analysis case, as shown in Fig. 33.11. The first of these was at the upper bass-side corner of the bridge (again to generate results comparable to the Bissinger data [2]). The other four were selected at each of the string-bridge interface points. These were selected to be used in future studies that may include measurements of the forces from the strings being transmitted to the bridge during normal operation (i.e. a musician playing the violin). All three degrees-of-freedom were included for each input point, bringing the total number of inputs to fifteen.

33.3 Results

33.3.1 FE Results for the Titian Stradivari Violin

The final results of the *Titian* Stradivari violin structural FE normal modes analysis is given in Table 33.4.

33.3.2 Corpus Modes (Signature Modes)

The most important modes of the violin structural FE are the three corpus flexural modes, shown in Figs. 33.12, 33.13, and 33.14. These are the corpus twisting mode known as the CBR (Center-Bout-Rhomboid) mode, and the two corpus bending modes, B1− and B1+. These involve flexure of the plates, and are the efficient radiators of sound in the open string frequency range of the violin (196–659 Hz), and are the structural signature modes [2].

33.3.3 Correlation Results of the Titian Stradivari Structural Model

The initial results of the *Titian* violin FE model were correlated with those from test data using the Modal Assurance Criterion (MAC). A plot of the MAC matrix is shown in Fig. 33.15. Note that string frequencies were removed from both sets. The color scale indicates MAC values from 0 (poor correlation, blue (dark in print version)) to 1 (good correlation, red (light in print version)). A magenta (white in print version) box has been added to the figure around the signature modes sub-matrix. These are the main modes of interest as they are the strongest radiators of sound, and are expected to be well captured in the experimental data.

The correlation results were updated to include all modifications and material updates made to the model. The final MAC matrix results are shown in Fig. 33.16. Again, string frequencies have been removed from both sets. The final mode pairs are given in Table 33.5; note that only mode pairs with MAC values greater than 0.6 are included. Overall the final correlation results are excellent. The average absolute percent frequency difference for the signature modes is 3.8 %. The average MAC value for the signature modes is 0.873.

Table 33.4 Summary of updated Titian Stradivari violin normal modes analysis

Mode #	Description	Frequency (Hz)
1	B0 (Tail IP)	158.9
2	B0 (Tail OP)	181.1
3	Lateral B0 (Tail IP)	223.5
4	B0 (FB bend)	227.2
5	Lateral B0 (Tail OP)	245.8
6, 7	1st G-string	195.0, 197.0
8, 9	1st D-string	292.2, 294.8
10, 11	2nd G-string	387.9, 393.0
12	CBR	427.3
13, 14	1st A-string	436.2, 442.5
15	B1−	452.5
16	B1+	529.8
17, 18	2nd D-string	587.5, 589.0
19, 20	3rd G-string	590.3, 593.3
21, 22	1st E-string	654.4, 657.5
23	Lateral FB	538.6
24	Neck-FB twist IP	633.6
25	Tail rock	650.8
26	Neck-FB twist OP	661.1

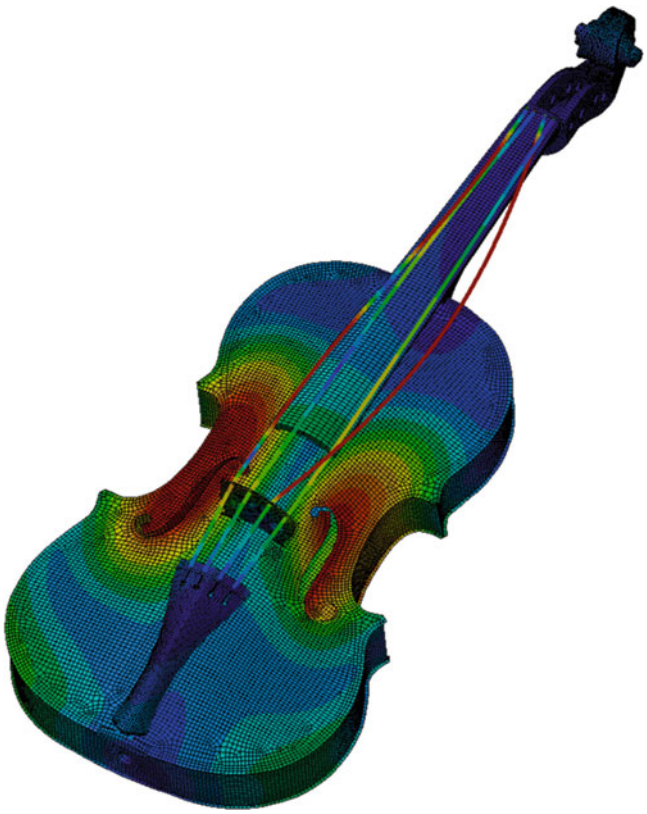

Fig. 33.12 CBR: 427.3 Hz

It is noted that the material properties of the *Titian* Stradivari violin FE model were updated to "tune" the modal frequencies. Updating was performed until the average percent difference for the three signature modes was below 5 %. A summary of the final material properties is given in Table 33.6.

Final mass of the full *Titian* Stradivari violin structural FE model was 323.2 g. The back plate of the model weighed 88.8 g, while the top plate + bass bar of the model weighed 48.1 g.

Fig. 33.13 B1−: 452.5 Hz

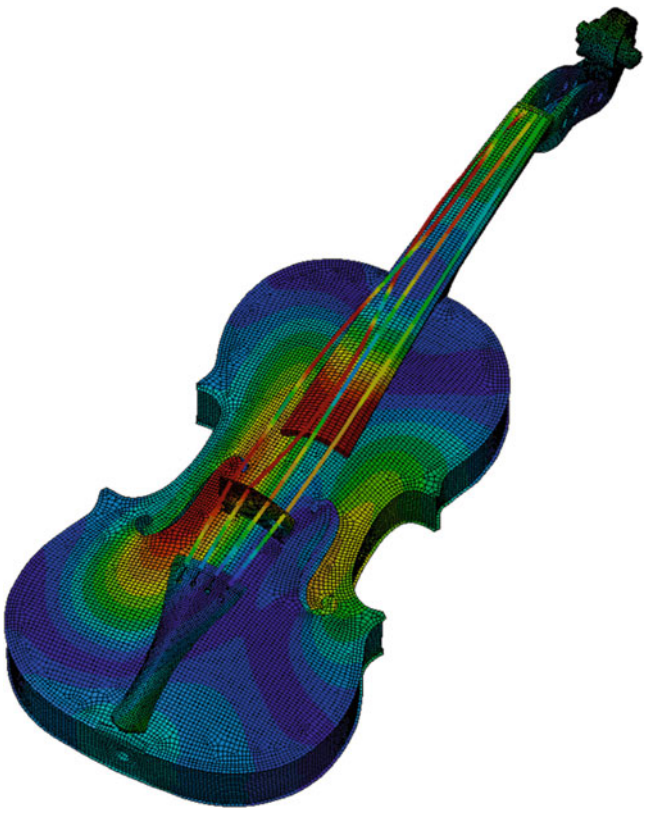

Fig. 33.14 B1+: 529.8 Hz

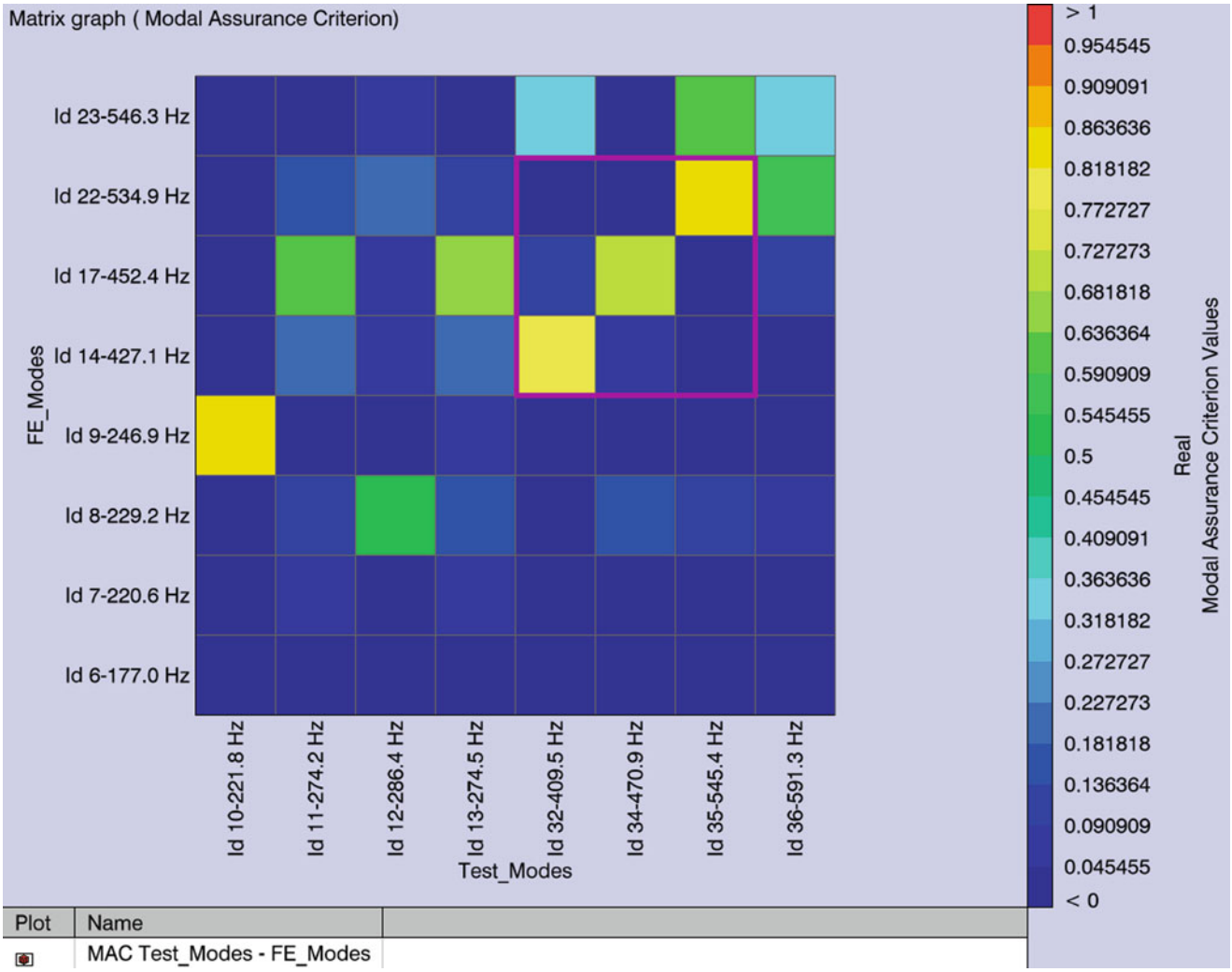

Fig. 33.15 Initial correlation results for the *Titian* violin

33.3.4 FEM Vibro-Acoustic Noise Transfer Function Analysis

The initial modal based vibro-acoustic noise transfer function case was set to calculate the transfer function for frequencies from 100 to 1,000 Hz with a 2 Hz increment. The Direct solver was used, rather than the iterative solver, due to the relatively small size of the model (<700,000 DOFs) and the complexity of a problem involving both interior and exterior domains.

The combined level multi-processing feature utilizes both frequency level and matrix level parallelization. This was used to speed up the solve time and to reduce total memory required. The system used for solving the model had two processor cores with two threads per processor.

The response of the point directly in front of the violin top plate was selected for comparison with the Bissinger test data. The transfer function (radiativity) magnitude for this point with respect to the lateral (X-direction) input at the upper bass-side corner of the bridge was extracted from each run and plotted against that of the Bissinger data [2].

Since the structural FE model was correlated with experimental modal data previously, the frequencies of peaks in the radiativity curve that are associated with structural FE modes are all within 5 % of those of the experimental data. The acoustic modes, A0 (275 Hz) and A1 (464 Hz), are of interest for verification of the vibro-acoustic model. The A1 peak is somewhat obfuscated by the B1− peak making it difficult to use as a reliable verifier. The A0 peak has a split in the experimental data of the *Titian* Stradivari violin, most likely due to a substructure mode. Despite this, the A0 peak is clearly visible, and can be used for updating the acoustic results. For comparison, the experimental peak in radiativity for A0 was 0.396 Pa/N.

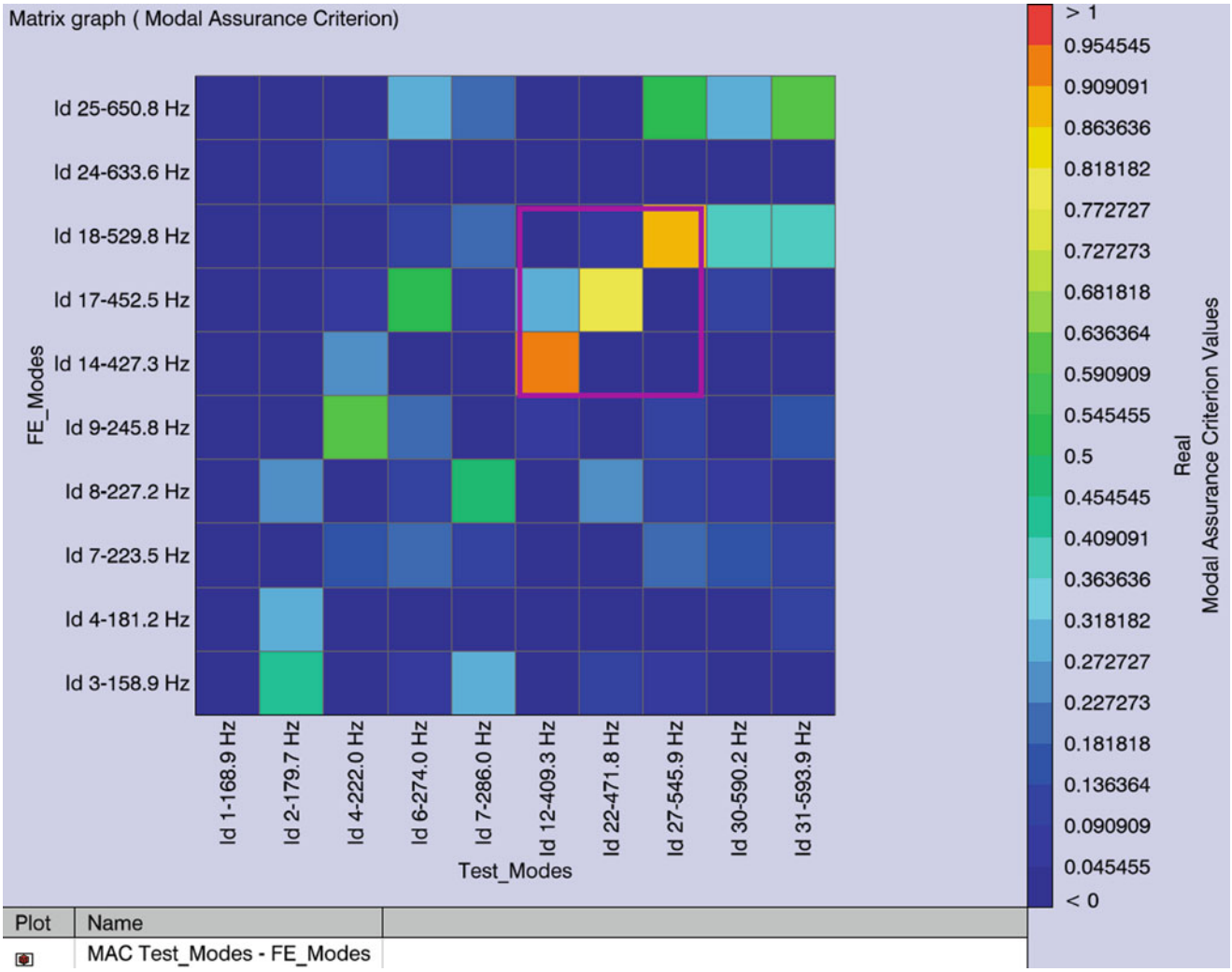

Fig. 33.16 Updated correlation results for the *Titian* violin

Table 33.5 Updated mode pair results for the *Titian* violin

Test id	Test freq (Hz)	FE id	FE freq (Hz)	MAC value	Freq diff (Hz)	Freq diff (% of test)
4	222	9	245.8	0.631	23.71	10.7
12	409.3	14	427.3	0.916	18.02	4.4
22	471.8	17	452.5	0.808	−19.25	−4.1
27	545.9	18	529.8	0.896	−16.08	−2.9
31	593.9	25	650.8	0.634	56.85	9.6

Table 33.6 Summary of final material properties for *Titian* Stradivari FE model

Component	Thickness (mm)	E1 (MPa)	E2 (MPa)	NU12	G12 (MPa)	G1Z (MPa)	G2Z (MPa)	RHO (kg/m^3)
Back plate	Variable	11,730	1,560	0. 424	892	505	265	570
Top plate	Variable	9,350	1,190	0.422	786	760	63.7	350

In the initial run the structural modes are left as is; that is, they are real normal modes and have no modal damping. The properties of air were kept as default real constant values, $c = 340$ m/s, $\rho = 1.225$ kg/m^3. The comparison of the radiativity result with experiment is given in Fig. 33.17. In almost all cases the peaks of the FE modes are sharper than those of the experiment, indicating that damping is important and needs to be included. The A0 mode is also considerably more prominent in the FE results (6.4 dB higher) than in the test data.

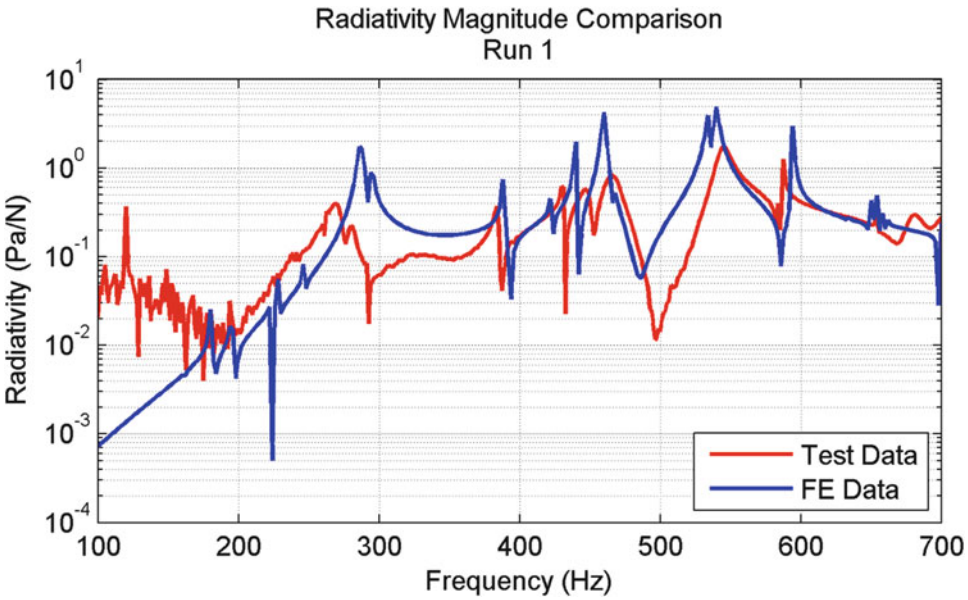

Fig. 33.17 Radiativity results comparison for point directly in front of violin top plate; real normal modes on structural FE; air properties constant real: $c = 340$ m/s, $\rho = 1.225$ kg/m^3

The properties of air are adjusted to include a loss factor in media. Skudrzyk shows that a loss factor, η, can be added to the speed of sound to make it complex [11]. This is shown in Eq. (33.4).

$$c = c_0 \left(1 + j\,\tfrac{\eta}{2}\right) \tag{33.4}$$

Lord also discusses this loss factor in terms of bending waves in a plate, and concludes that for small values of damping ($\zeta \leq 0.1$) this loss factor is approximately proportional to the damping factor, ζ [12]. This proportionality is given in Eq. (33.5).

$$\eta \cong 2\zeta \tag{33.5}$$

In the experimental data of the *Titian* Stradivari violin the radiativity has a split in the A0 peak. This is most likely due to a local structure mode of either the tail piece or fingerboard; however, since no response points were measured on either of these sub-structures, it is difficult to curve fit this area reliably, and the damping factor estimate would be particularly sensitive.

The average damping factor of the A0 mode for all 14 violins in the VIOCADEAS database [4] is 2.12 %. The loss factor in the air property was thus adjusted. In the final run the speed of sound was $c = 340 + j8$ m/s. The structural modal damping, the string modes were undamped, while all others had an estimated modal damping applied.

The comparison of the transfer function of the point over the top with respect to the bass-side bridge input for this final analysis run compared to the experimental data is given in Fig. 33.18. The FE and test curves follow the same trend. Structural modes all have approximately the same shape (again, structural damping is realistic). The peak of the predicted A0 mode is now only 1.45 dB above that of the test.

The predicted frequency of the A0 mode is consistently above that of test by 6.8 % for all four runs; this could be a function of the air density, or related to sound post stress loading [13, 14].

33.4 Conclusions

Based on the results of these analyses, the coupled vibro-acoustic FEM model of the *Titian* Stradivari violin is an excellent representation of the real structure. This model was created by measuring the structural geometry and density from CT scans of the actual instrument. Correlation between the experimental data and the initial FE models was used to compare the modal behavior, and the material properties in the models were iterated to determine a set of parameters that reflect the dynamic behavior of the real instruments. The structural model was updated so that the first several modes were within 5 % of the experimental modal frequencies, and all MAC values for mode pairs of interest were above 0.6.

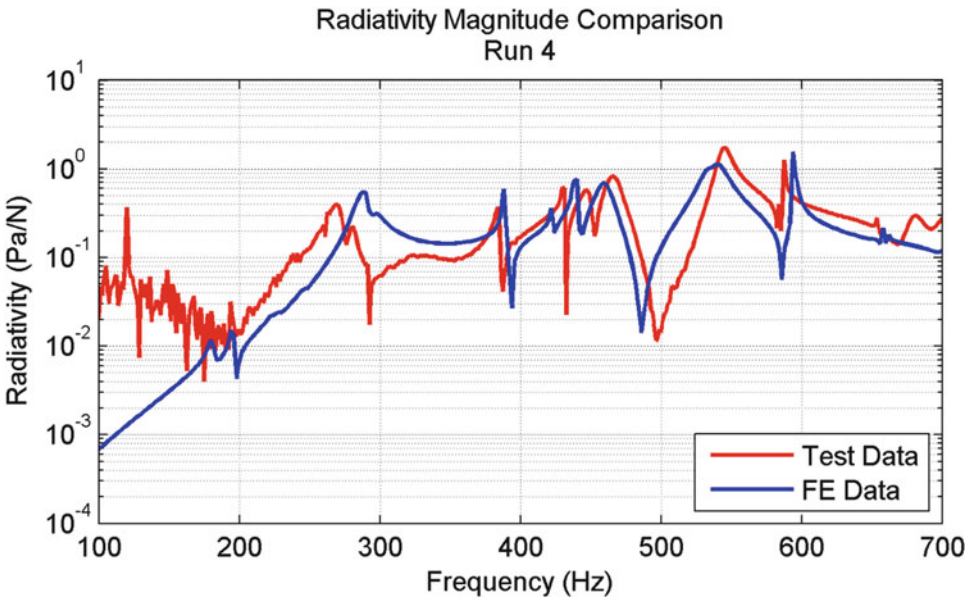

Fig. 33.18 Radiativity results comparison for point directly in front of violin top plate; modal damping added to structural modes (except string modes); air properties complex: $c = (340 + j8)$ m/s, $\rho = 1.225$ kg/m^3

Most importantly structural and acoustic damping characteristics were taken from a 14 violin experimental study [2]. These were incorporating into a fully coupled vibro-acoustic model of the *Titian* Stradivari violin using the latest acoustic FEM techniques.

It was shown that by including all these details, the vibro-acoustic behavior of the *Titian* Stradivari violin is accurately predicted. Predicted structural mode frequencies were all within 5 % of the experimentally measured modes. The main acoustic mode, A0, of the *Titian* Stradivari was predicted within 7 % of the experimental result, and its associated peak in the radiativity magnitude was within 1.5 dB.

References

1. Pyrkosz M, Van Karsen C, Bissinger G (2010) Converting CT scans of a stradivari violin to a FEM. In: Proceedings of the 28th international modal analysis conference, Jacksonville, February 2010
2. Bissinger G (2008) Structural acoustics of good and bad violins. J Acoust Soc Am 124(3):1764–1773
3. Bissinger G (2005) A unified materials-normal mode approach to violin acoustics. Acustica 91:214–228
4. Bissinger G (2008) Structural acoustics model of the violin radiativity profile. J Acoust Soc Am 124(6):4013–4023
5. Knott GA (1987) A modal analysis of the violin using MSC/NASTRAN and PATRAN. M.S. Thesis, Naval Postgraduate School. Available through NTIS website (March 1987)
6. "Thickness Contour Maps" by Jeffrey Loen with Violin specification and thickness measurements by S. Zygmuntowicz, Strad3D (2009)
7. Allemang RJ (2002) The modal assurance criterion (MAC): twenty years of use and abuse. In: Proceedings of the international modal analysis conference, Los Angeles, February 2002
8. Heylen W, Lammens S, Sas P (1998) Modal analysis theory and testing. Katholieke Universiteit Leuven, Department of Mechanical Engineering, Division of Production Engineering, Machine Design and Automation, Leuven
9. Desmet W et al (1998) Numerical acoustics – theoretical manual. LMS International
10. Hong K et al (2008) LMS International A next generation solution for functional performance engineering – LMS Virtual.Lab Acoustic Training
11. Skudrzyk E (1972) The foundation of acoustics: basic mathematics and basic acoustics. Springer, New York, pp 319–322
12. Lord H, Gatley W, Evensen H (1980) Noise control for engineers. Krieger Pub. Co., Malabar, pp 258–263
13. Meinl H (1937) On the frequency curves of violins. Akust Z 2:22–33. Translated by Fan C (2007)
14. Bissinger G (1995) Some mechanical and acoustical consequences of the violin soundpost. J Acoust Soc Am 97:3154–3164